



Quantitative modeling of the variation in stress–strain response of shape memory alloys in partial phase transformed state

G JAYABHARATH REDDY* and S MANIPRAKASH

Department of Mechanical Engineering, Indian Institute of Information Technology Design and Manufacturing Kurnool, Kurnool, India
e-mail: guredyjayabharath@gmail.com; smp@iiitk.ac.in

MS received 24 August 2023; revised 7 November 2023; accepted 7 December 2023

Abstract. This work proposes a thermodynamic-based constitutive model for shape memory alloy, which captures the gradual variation in stress–strain response from the shape memory effect to the pseudoelastic effect. The present model also provides a framework for modeling various other responses, such as strain temperature hysteresis and thermally induced strain recovery effect. The model classifies the different phases of the material, such as twinned martensite, detwinned martensite, and austenite, and the mix of these phases using only two internal variables, namely austenite volume fraction and inelastic martensite strain. The proposed model shows that introducing two independent yield conditions corresponding to each internal variable is sufficient to describe all the phase transformations. After presenting the theoretical framework of the model, the procedure for numerical implementation has been discussed. The simulation shows the gradual variation in the stress–strain curve at different temperatures in the phase transformation range and is observed to have an adequate quantitative agreement with the experimental data. The model is further implemented for different shape memory alloys to show the possibility of the generalized framework for this class of materials. In addition, the capability of simulating other phenomena of SMA, such as strain response for thermal loading at constant stress and the complete response of strain recovery in shape memory behavior, is also presented.

Keywords. Shape memory alloys; constitutive model; martensitic phase transformation.

1. Introduction

Among various functional materials, shape memory alloys (SMAs) can recover significant strain of up to 7% [1]. The recovery is either due to the temperature rise or just due to the unloading of the stress. These phenomena are known as the shape memory effect and the pseudoelastic effect, respectively. Due to this unique behavior, it is used in many engineering applications. The shape memory effect of the material is utilized in temperature controls such as air conditioners, thermostatic mixing valves, etc. [2]. The material has also been used as an actuator in automotive and aerospace applications [3]. In biomedical applications, shape memory alloys are used, such as implantation in orthodontics, minimally invasive surgery, etc. [4]. Because of the material's ability to perform as both sensor and actuator, SMAs are used as the intelligent controller. A novel sun-tracking mechanism using SMA wire and modular stiffness control structures are examples of such a smart controller [5, 6]. Recently, the material has been used in the applications of soft robotics [7–9].

The underlying mechanism behind these phenomena is the phase transition behavior of the material. In the shape memory effect, when the material is loaded at low temperatures, it transforms from twinned to detwinned martensite providing the deformation. When this is followed by the rise in temperature, it leads to austenite formation with simultaneous strain recovery. Apart from this, the material exhibits pseudoelastic behavior due to the phase transformation between austenite and martensite under the applied stress. To effectively utilize the potential of SMAs, a mathematical model describing the behavior is essential. Such models can be done at different length scales, from lattice or crystal level to macroscopic level of the alloy. Micromechanical models account for microstructural effects such as crystal structure change, residual stress during transformation, and interface motion which influence macroscopic behavior. For a detailed review of micromechanical models, see [10]. Although accurate, this approach is associated with high computing costs for modeling the bulk material.

The martensite transformation in bulk materials is described by macroscopic phenomenological models, which can be classified into phenomenological models and models with thermodynamic considerations [11, 12]. The

*For correspondence
Published online: 23 March 2024

earlier constitutive models employed mathematical functions to describe the material's response using a phase diagram. For instance, a one-dimensional model proposed by Tanaka and Liang utilized exponential and cosine functions to describe the phase transformation kinetics [13, 14]. Brinson proposed a modified phase diagram by splitting the martensite volume fraction into temperature-induced and stress-induced martensite to describe the twinning behavior [15]. Based on a similar kinetics approach a model was proposed for arbitrary thermal and mechanical loading conditions [16]. To model the difference in elastic properties between martensite and austenite, thermodynamically consistent non-constant material functions are defined based on first principles [17]. These models have the advantage of simplicity without an iterative procedure in a stress-based approach. In a similar model, this advantage has been extended in the strain-based model by using polynomial kinetic equations [18].

Another modeling approach uses a generalized plasticity framework. In this regard, a simple one-dimensional model was proposed by Aurruchio [19] with three internal variables. Using different evolution equations for forming austenite, single and multiple variant martensite, the model can describe the pseudoelasticity and shape memory effect along with multiple cycle loading. A similar model has been proposed to accommodate multiple as well as partial loading and unloading conditions [20]. A thermodynamic-based strain-driven model was proposed by Souza *et al* [21] with a deviatoric strain tensor as an internal variable. Auricchio *et al* [22] extended this work to a boundary value problem. With this framework, the model was tested for uni-axial and multi-axial non-proportional loading to mimic the loading condition of some SMA applications, such as a spring actuator, a self-expanding stent, and a coupling device for vacuum tightness. Based on a stress-based thermodynamic framework, a 3-D model has been proposed by Boyd and Lagoudas [23]. This work presents an explicit form of Gibbs free energy with martensite volume fraction and total irreversible strain as internal variables. Qidwai and Lagoudas [24] extended this to include the principle of maximum dissipation and various transformation functions are analyzed for a generalized phase transformation function which can accommodate for volumetric change and asymmetric behavior. The above models do not explicitly differentiate between twinned and detwinned martensite. To account for the martensite reorientation, a model introducing three internal variables has been proposed [25]. This work accounts for three distinct phases with twinned and detwinned martensite separately. To reduce the computational complexity of the Souza model, a model was proposed by avoiding predictor–corrector type approach [26].

Similar models were proposed using additional internal variants to include transformation-induced plasticity and reorientation under non-proportional loading [27, 28]. It is observed that the material has an additional intermediate

R-phase during the forward transformation [29]. Some models were proposed incorporating this independent phase transformation [30, 31]. As many applications of SMA undergo repetitive loading, it is essential to account for functional degeneration and fatigue behavior [32]. Some models were proposed to describe functional fatigue by accounting for transformation-induced plasticity, change in transformation stress, and structural fatigue with critical value for internal damage variables [33, 34]. In one of the recent works by Alsawalhi *et al* [35], multiple transformation functions are reduced to a single function to represent all the phase transformation behavior. In addition to irreversible strain, the framework uses transformation entropy as an internal variable.

Some works focused on rate dependent effect of SMA. It is observed that the behavior of alloy is dependent on strain rate, which is mainly due to the production of latent heat during phase transformation [36]. In Ref. [37, 38], the authors have considered this effect by incorporating phase transformation and heat transfer equations. This effect is accounted for from this approach by introducing an additional internal variable [39]. For the SMA spring actuator application, a model [40] has been proposed to derive the relation between the twist and torque. In this thermodynamic-based approach, torque is considered a state variable instead of stress. However, this approach has limitations during the analysis of SMA springs with large spring index [41].

Experimental validation of models present in commercial FEA packages reveals a requirement for a simple and comprehensive constitutive model [42]. Many models proposed in the literature usually have a complex formulation for individual phase transformation and evolution laws depending on the loading direction. They also have multiple model parameters requiring calibrations with the experimental data. Some models were proposed in a framework that doesn't require the prescription of the type of transformation in advance along with a minimal set of variables [43], and the results were limited only to a qualitative comparison with the experimental data. Most of the proposed models capture the behavior of complete phase transformation. However, in certain applications, the material undergoes a partial transformation [44]. Therefore, there is still a requirement for a model that can closely capture the material behavior under complex thermomechanical loading, particularly in the phase transformation regime. In addition to that, the model has to be easily implementable from the application engineers' perspective.

With this motivation, in this study, we propose a thermodynamic based new constitutive model to describe all three-phase transformations. The proposed model has captured the gradual variation in stress–strain behavior under different temperatures, which fall under the range of phase transition temperatures. Unlike many other models, the proposed model doesn't require an a priori knowledge of phase transformations. With this framework, the proposed

model can account for complex thermomechanical loading, which is very helpful for actuator applications. The proposed work has described phases such as austenite, twinned, and detwinned martensite using two internal variables. The phase transformation processes, such as forward, reverse phase transformation, stress-induced transformations, and reorientation of twinned to detwinned martensite can be described in terms of the variation of the internal variables. This description also helps in modeling the partial transformation behavior of the alloy. Such a partial transformation is expected in the application of actuators. Though the work focuses on a rate-independent model, it can be easily extended to include the rate-dependent effects. The thermodynamic approach of the model helps in calculating the energy dissipation. Thus the model can be utilized to calculate the structural and functional fatigue of the material by equating the dissipation to the degradation in the material. The organization of this work is as follows the constitutive model is described in section 2 along with the proposed Gibbs free energy. The evolution equations required for phase transformation are discussed in section 3. The numerical implementation of the model is discussed in section 4. Finally, the results for different loading conditions and discussion are explained in section 5.

2. Constitutive model

This section describes the proposed 1D constitutive model for Shape Memory Alloy. In this stress-based model, the state variable of the alloy is taken to be stress σ and temperature T . Strain ε , which is a conjugate variable to stress, is additively decomposed into elastic and inelastic parts as follows

$$\varepsilon = \varepsilon^e + \varepsilon^{in}, \quad (1)$$

where, ε^e represents the elastic part of the strain and ε^{in} represents the inelastic part of the strain. The inelastic part is written as a function of two internal variables, which are the volume fraction of austenite v^a and the inelastic martensite strain ε^{mt} . The meaning of v^a is straightforward; however, the meaning of ε^{mt} can be understood as the inelastic strain exerted in the martensite fraction such that the total inelastic strain can be written as $\varepsilon^{in} = \varepsilon^{mt}(1 - v^a)$. Therefore, the total strain can be written as

$$\varepsilon = \varepsilon^e + \varepsilon^{mt}(1 - v^a). \quad (2)$$

The constitutive model is proposed based on continuum thermodynamic considerations by satisfying the satisfying the Clausius–Duhem inequality given by

$$\rho T \dot{s} - \rho \dot{u} + \sigma \dot{\varepsilon} - \frac{q \nabla T}{T} \geq 0 \quad (3)$$

where T , ρ , u , s are temperature, density, specific internal energy, specific entropy and σ , ε , q are stress, strain, and

heat flux respectively. With the assumption of uniform temperature distribution the last term of the above equation can be neglected, the dissipation (\mathcal{D}) inequality can be rewritten in terms of Gibbs free energy (G), a thermodynamic potential defined as $G = u - \frac{\sigma \varepsilon}{\rho} - T s$, as

$$\mathcal{D} = -\rho \dot{G} - \dot{\sigma} \varepsilon - \rho s \dot{T} \geq 0 \quad (4)$$

By considering Gibbs free energy as a function of external and internal state variables, i.e., $G = G(\sigma, T, \varepsilon^{mt}, v^a)$ the time derivative of G is given as

$$\dot{G}(\sigma, \varepsilon^{mt}, v^a, T) = \frac{\partial G}{\partial \sigma} \dot{\sigma} + \frac{\partial G}{\partial \varepsilon^{mt}} \dot{\varepsilon}^{mt} + \frac{\partial G}{\partial v^a} \dot{v}^a + \frac{\partial G}{\partial T} \dot{T} \quad (5)$$

Substituting (5) into (4), gives

$$\begin{aligned} \mathcal{D} = & \left[-\rho \frac{\partial G}{\partial \sigma} - \varepsilon \right] \dot{\sigma} + \left[-\rho \frac{\partial G}{\partial T} - \rho s \right] \dot{T} \\ & - \rho \frac{\partial G}{\partial \varepsilon^{mt}} \dot{\varepsilon}^{mt} - \rho \frac{\partial G}{\partial v^a} \dot{v}^a \geq 0 \end{aligned} \quad (6)$$

Since the rate of external variables $\dot{\sigma}$ and \dot{T} can be arbitrary, the coefficient of these terms has to be vanished [45]. This condition leads to the following state equations.

$$\varepsilon = -\rho \frac{\partial G}{\partial \sigma} \quad (7)$$

$$s = -\frac{\partial G}{\partial T} \quad (8)$$

$$\mathcal{D} = -\rho \frac{\partial G}{\partial \varepsilon^{mt}} \dot{\varepsilon}^{mt} - \rho \frac{\partial G}{\partial v^a} \dot{v}^a \geq 0 \quad (9)$$

To establish the state equation for the behavior of SMA, the following form of Gibbs free energy is proposed. The free energy potential is additively decomposed into the reversible part, which comprises the first three terms and the irreversible part with the remaining three terms as follows

$$\begin{aligned} G(\sigma, \varepsilon^{mt}, v^a, T) &= G^r(\sigma, \varepsilon^{mt}, v^a, T) + G^{ir}(\varepsilon^{mt}, v^a, T) = \frac{-1}{2\rho} \sigma^2 S(v^a) \\ &- \frac{1}{\rho} \sigma [\alpha(v^a)(T - T_0) + \varepsilon^{mt}(1 - v^a)] \\ &+ c(v^a) \left[(T - T_0) - \ln \left(\frac{T}{T_0} \right) \right] \\ &+ \frac{a}{\rho} \left[\frac{\varepsilon^{mt}}{\varepsilon_s^{mt}} \cdot \tanh^{-1} \left(\frac{\varepsilon^{mt}}{\varepsilon_s^{mt}} \right) + \frac{1}{2} \ln \left| 1 - \left(\frac{\varepsilon^{mt}}{\varepsilon_s^{mt}} \right)^2 \right| \right] \\ &+ \frac{b}{2\rho} [(2v^a - 1) \tanh^{-1}(2v^a - 1) \\ &+ \frac{1}{2} \ln |1 - (2v^a - 1)^2|] + \frac{c_1 \ln(c_2 - v^a)}{\rho} (T - T^\circ) \end{aligned} \quad (10)$$

where T_0 represents the entropy value, temperature, and

internal energy, respectively. The parameters ε_s^{mt} , a , b , c_1 , c_2 , T° represents the model parameters. ε_s^{mt} can be interpreted as the maximum inelastic strain the material could undergo in the martensite phase. The variables S , c , α represent compliance, heat capacity, and thermal expansion coefficient of the material, respectively. Motivated by the work on ferroelectrics [46, 47], the free energy is chosen such that internal variables are bounded in the range given by $0 < v^a < 1$ and $|\varepsilon^{mt}| < \varepsilon_s^{mt}$. The effective material properties in terms of pure phases are given as

$$\begin{aligned} S(v^a) &= S^M + v^a(S^A - S^M) = S^M + v^a \Delta S \\ c(v^a) &= c^M + v^a(c^A - c^M) = c^M + v^a \Delta c \\ \alpha(v^a) &= \alpha^M + v^a(\alpha^A - \alpha^M) = \alpha^M + v^a \Delta \alpha \end{aligned}$$

where $(\cdot)^M$ and $(\cdot)^A$ represent a particular material property in the martensite and austenite phase, respectively.

By using (7) the strain can be defined in terms of state variables as

$$\begin{aligned} \varepsilon &= -\rho \frac{\partial G}{\partial \sigma} = \sigma S(v^a) + \alpha(v^a)(T - T_0) + \varepsilon^{mt}(1 - v^a) \\ &\approx \sigma S(v^a) + \varepsilon^{mt}(1 - v^a) \end{aligned} \quad (11)$$

The above approximation is obtained by ignoring the effect of thermal expansion compared to the last term, which is the inelastic term. By comparing with (1), we can identify the first term in (11) represents the elastic part of the strain. By substituting the proposed Gibbs potential in the dissipation inequality condition (9) and noting that $\Delta c = 0$, we obtain

$$\begin{aligned} \mathcal{D} &= \left[\sigma(1 - v^a) - \rho \frac{\partial G^{ir}}{\partial \varepsilon^{mt}} \right] \dot{\varepsilon}^{mt} \\ &+ \left[\frac{\sigma^2}{2} \Delta S - \sigma \varepsilon^{mt} - \rho \frac{\partial G^{ir}}{\partial v^a} \right] \dot{v}^a \geq 0 \end{aligned} \quad (12)$$

The coefficient of the rate of internal variables represents the respective conjugate thermodynamic forces. To calculate the strain for the given stress and the temperature using (11), the internal variables such as ε^{mt} and v^a have to be calculated. In the following section, the evolution equation for the internal variables will be presented. These equations are derived such that the above dissipation inequality is satisfied.

3. Evolution of internal variables

For the evolution of ε^{mt} , a condition has been introduced in terms of a yield function ϕ^ε . In order to satisfy the dissipation inequality, the yield function is chosen such that the conjugate thermodynamic force of ε^{mt} per martensite frac-

tion exceeds a critical value, and the evolution will happen. Therefore, the yield function can be written as

$$\phi^\varepsilon = \left| \sigma - \frac{\beta^\varepsilon}{1 - v^a} \right| - \sigma_c \leq 0 \quad (13)$$

where, σ_c represents the critical stress value and $\beta^\varepsilon = \rho \partial G^{ir} / \partial \varepsilon^{mt}$. From the above equation, we can see that once the conjugate thermodynamic force exceeds a threshold limit, ε^{mt} will change. This represents the reorientation from twinned to detwinned martensite. It can also be observed that when the material is completely austenite, such transformation is not possible. The relation between β^ε and ε^{mt} can be obtained from the proposed Gibb's potential as

$$\varepsilon^{mt} = \varepsilon_s^{mt} \tanh\left(\frac{\beta^\varepsilon}{a}\right) \quad (14)$$

Since there is a one-to-one relation between ε^{mt} and β^ε , the updated internal variable can be obtained by updating β^ε . Therefore, β^ε is being treated as a stored value in the simulation procedure.

Similarly, for the evolution of v^a , another yield function ϕ^v has been introduced as

$$\begin{aligned} \phi^v &= \left| \frac{\sigma^2 \Delta S}{2} - \sigma \varepsilon^{mt} - \rho \frac{\partial G^{ir}}{\partial v^a} \right| - T_c \leq 0 \\ \phi^v &= \left| T - T^\circ + \frac{\sigma^2 \Delta S}{2C} - \frac{\sigma \varepsilon^{mt}}{C} - \frac{\beta^T}{C} \right| - T_c \leq 0 \end{aligned} \quad (15)$$

where, T_c represents the critical temperature value and $\beta^T = \rho \partial G^{ir} / \partial v^a + C(T - T^\circ)$ and $C = \frac{c_1}{(c_2 - v^a)}$. From this definition of β^T , using Gibb's free energy, we can write a one-to-one relation between β^T and v^a as

$$v^a = 0.5 \left[1 + \tanh \frac{\beta^T}{b} \right] \quad (16)$$

Therefore, β^T will be stored for computational purpose, and the austenite volume fraction will be calculated using the above equation. The yield criteria given in equation (15) represents that the combination of stress and temperature exceeds a threshold limit, and a transformation happens between the austenite and martensite phases. T° can be interpreted such that under stress-free condition, T° is the average value of austenite start/finish temperature and martensite start/finish temperature. The term $\sigma^2 \Delta S / 2C$ influences the transformation temperature under the application of stress. The term $\sigma \varepsilon^{mt} / C$ gets activated upon applying stress only when there is a presence of martensite transformation strain. Due to the presence of this term, pseudo-elastic stress-strain curves show different hardening behavior between loading and unloading conditions. This behavior is also observed in the experimental data, which is discussed in the result section.

4. Time integration

For a numerical simulation, the applied stress and temperature are discretized into many load steps. The variables corresponding to the current load step are denoted with the subscript $(n + 1)$. At the current load step, for a given σ_{n+1} and T_{n+1} , β_{n+1}^e , β_{n+1}^v and ε_{n+1} has to be calculated provided β_n^e and β_n^T are known. In order to do this, equation (15) can be written as

$$\phi^v = \left| T_{n+1} - T^\circ + \frac{\sigma_{n+1}^2 \Delta S}{2 C_{n+1}} - \frac{\sigma_{n+1} \varepsilon_{n+1}^{mt} (\beta_{n+1}^e)}{C_{n+1}} - \frac{\beta_{n+1}^T}{C_{n+1}} \right| - T_c \leq 0 \tag{17}$$

Similarly, the equation (13) can be written as

$$\phi^e = \left| \sigma_{n+1} - \frac{\beta_{n+1}^e}{1 - v_{n+1}^a (\beta_{n+1}^T)} \right| - \sigma_{c_{n+1}} \leq 0 \tag{18}$$

To update the internal variables, the above two inequality constraints have to be satisfied simultaneously. The material parameters C_{n+1} and $\sigma_{c_{n+1}}$ are updated simultaneously with the internal variable v^a . To perform this update, a trial value of yield functions ϕ_{tr}^v and ϕ_{tr}^e are introduced as

$$\phi_{tr}^v = \left| T_{n+1} - T^\circ + \frac{\sigma_{n+1}^2 \Delta S}{2 C_{n+1}} - \frac{\sigma_{n+1} \varepsilon_{n+1}^{mt} (\beta_{n+1}^e)}{C_{n+1}} - \frac{\beta_n^T}{C_{n+1}} \right| - T_c \tag{19}$$

$$\phi_{tr}^e = \left| \sigma_{n+1} - \frac{\beta_n^e}{1 - v_{n+1}^a (\beta_{n+1}^T)} \right| - \sigma_{c_{n+1}} \tag{20}$$

By calculating these two variables, the updating procedure can be performed by solving the following two equations.

$$\beta_{n+1}^e = \beta_n^e + \langle (1 - v^a (\beta_{n+1}^T)) \phi_{tr} (\beta_{n+1}^T) \rangle \text{sgn} \left(\sigma_{n+1} - \frac{\beta_n^e}{1 - v^a (\beta_{n+1}^T)} \right) \tag{21}$$

$$\beta_{n+1}^T = \beta_n^T + C_{n+1} \langle \phi_{tr}^v \rangle \text{sgn} \left(T_{n+1} - T^\circ - \frac{1}{2 C_{n+1}} \sigma_{n+1}^2 \Delta S - \frac{\sigma_{n+1} \varepsilon_{n+1}^{mt} (\beta_{n+1}^e)}{C_{n+1}} - \frac{\beta_n^T}{C_{n+1}} \right) \tag{22}$$

where $\langle \cdot \rangle$ Macaulay's bracket which is defined as $\langle \cdot \rangle = (\cdot + |\cdot|)/2$. The above two equations are nonlinear and need to be solved using an iterative procedure. The pseudocode for the algorithm is given in table 1.

5. Results

In this section, the proposed model is simulated under three types of thermomechanical loading conditions. The simulations are chosen such that they describe different properties of the alloy. These phenomena are discussed with the variation of internal variables along the loading conditions. The model parameters are judiciously chosen such that the simulation results are in good agreement with the experimental data. To show the robustness of the model in capturing the behavior of various SMA materials, validation with experimental data has been performed just by varying the model parameters for four different materials without modifying the framework of the model.

5.1 Stress strain behaviour

Initially, the stress–strain behavior at different operating temperatures is analyzed. Also, the simulation results are compared with experimental data available in the literature. For this, the isothermal tests done on NiTi Alloy (50.1% Ni) by Shaw and Kyriakides [48] are simulated. The model parameters chosen for the analysis are given in table 2. Some critical material parameters like elastic modulus (E_A & E_M) and maximum available transformation strain (ε_s^{mt}) are taken from the experimental uniaxial test data. The initial state of the alloy is different for different operating temperatures, given in terms of internal variables. The initial state can be incorporated into the model by subjecting the alloy to an initial hypothetical loading condition from a reference state. This is done by raising the temperature from a small value to the operating temperature at zero stress. The reference state is given by a zero volume fraction of austenite and zero martensite inelastic strain ε^{mt} . The loading curve of this phase is given from t_0 to t_1 in figure 1. Once the operating temperature T_{opt} value is reached, it is maintained while the stress ramps up to σ_{max} at $t = t_2$. Then, the stress ramps to zero without changing the temperature value. This part of loading is given in the interval between t_2 and t_3 as shown in figure 1.

During the interval between $t = t_0$ to $t = t_1$, only the temperature is raised, and the stress remains zero. This results in the increase of the volume fraction of austenite v^a while maintaining ε^{mt} to be zero. The change of these internal variables is shown in figure 2. The value of v^a begins to change from zero once it reaches a certain temperature value. This represents the beginning of the phase change from martensite to austenite. The continuation of the rise in temperature increases the v^a until the temperature reaches T_{opt} . The simulation results show that the value of v^a at $t = t_1$ depends on the operating temperature. This represents the phase of the material for which the stress–strain behavior is simulated. Between t_1 and t_2 , once the stress value reaches a critical limit, ε^{mt} begins to increase. At that moment, we could also note the decrease in v^a . This

Table 1. Algorithmic sketch for shape memory alloy model.

Given : σ_{n+1} , T_{n+1} , β_n^ε and β_n^v

Compute :

set $k = 1$, $\beta_{n+1}^\varepsilon = \beta_n^\varepsilon$, $\beta_{n+1}^v = \beta_n^v$
 set $\varepsilon_k^{mt} = \varepsilon^{mt}(\beta_{n+1}^\varepsilon)$, $\varepsilon_{k+1}^{mt} = \varepsilon_k^{mt} + tol$

while : $tol \leq |\varepsilon_{k+1}^{mt} - \varepsilon_k^{mt}|$

$$\phi_{tr}^v = \left| T_{n+1} - T^\circ + \frac{\sigma_{n+1}^2 \Delta S}{2C_{n+1}} - \frac{\sigma_{n+1} \varepsilon^{mt}(\beta_{n+1}^\varepsilon)}{C_{n+1}} - \frac{\beta_n^T}{C_{n+1}} \right| - T_c$$

$$\beta_{n+1}^T = \beta_n^T + C_{n+1} \langle \phi_{tr}^v \rangle \text{sgn}(T_{n+1} - T^\circ - \frac{1}{2C_{n+1}} \sigma_{n+1}^2 \Delta S - \frac{\sigma_{n+1} \varepsilon^{mt}(\beta_{n+1}^\varepsilon)}{C_{n+1}} - \frac{\beta_n^T}{C_{n+1}})$$

$$\phi_{tr}^\varepsilon = \left| \sigma_{n+1} - \frac{\beta_n^\varepsilon}{1 - \nu^a(\beta_{n+1}^T)} \right| - \sigma_{c_{n+1}}$$

$$\beta_{n+1}^\varepsilon = \beta_n^\varepsilon + \langle (1 - \nu^a(\beta_{n+1}^T)) \phi_{tr}^\varepsilon(\beta_{n+1}^T) \rangle \text{sgn}(\sigma_{n+1} - \frac{\beta_n^\varepsilon}{1 - \nu^a(\beta_{n+1}^T)})$$

$$\varepsilon_{k+1}^{mt} = \varepsilon_s^{mt} \tanh\left(\frac{\beta_{n+1}^\varepsilon}{a}\right)$$

$$k = k + 1$$

end

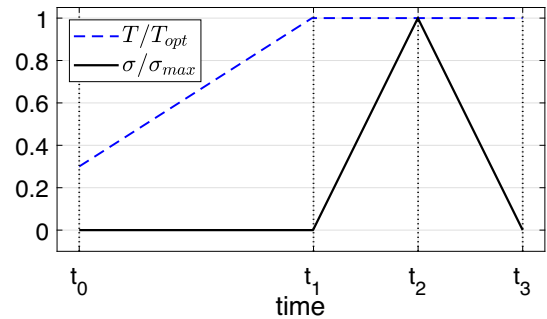
$$\nu^a = 0.5 \left[1 + \tanh\left(\frac{\beta_{n+1}^T}{b}\right) \right]$$

$$\varepsilon_{n+1} = S(\nu^a) \sigma_{n+1} + (1 - \nu^a) \varepsilon_{k+1}^{mt}$$

Table 2. Model parameters used in numerical simulations For NiTi Alloy(50.1% Ni).

Parameter	Value	Unit
$S_A = 1/E_A$	1/62.701	GPa^{-1}
$S_M = 1/E_M$	1/30.591	GPa^{-1}
T_c	6	K
σ_c	$(1 - \nu) \times 135 + \nu \times 435$	MPa
T^0	299.5	K
c_1	0.7	$MPa K^{-1}$
c_2	3.4	–
ε_s^{mt}	0.05	–
a	80	MPa
b	6	K

behavior represents stress-induced martensite transformation. During the stress unloading between t_2 and t_3 , the austenite volume fraction increases again while the ε^{mt} decreases. The significance of this change during the unloading depends on the operating temperature. At low T_{opt} , the change is insignificant and shows a behavior similar to plastic material. At high T_{opt} , the change in the

**Figure 1.** Stress and Temperature loading for Shape memory alloy.

internal variable is significant, resulting in the material's pseudoelastic response.

The stress–strain behavior of the simulation results, along with the comparison of experimental data, is given in figure 3. The experimental data shows the variation in the stress–strain behavior from the shape memory effect to the pseudoelastic effect for varying operating temperatures. The simulation result captures this behavior very well. The results of the evolution of internal variables show that the material is in a partial phase-transformed state before it is

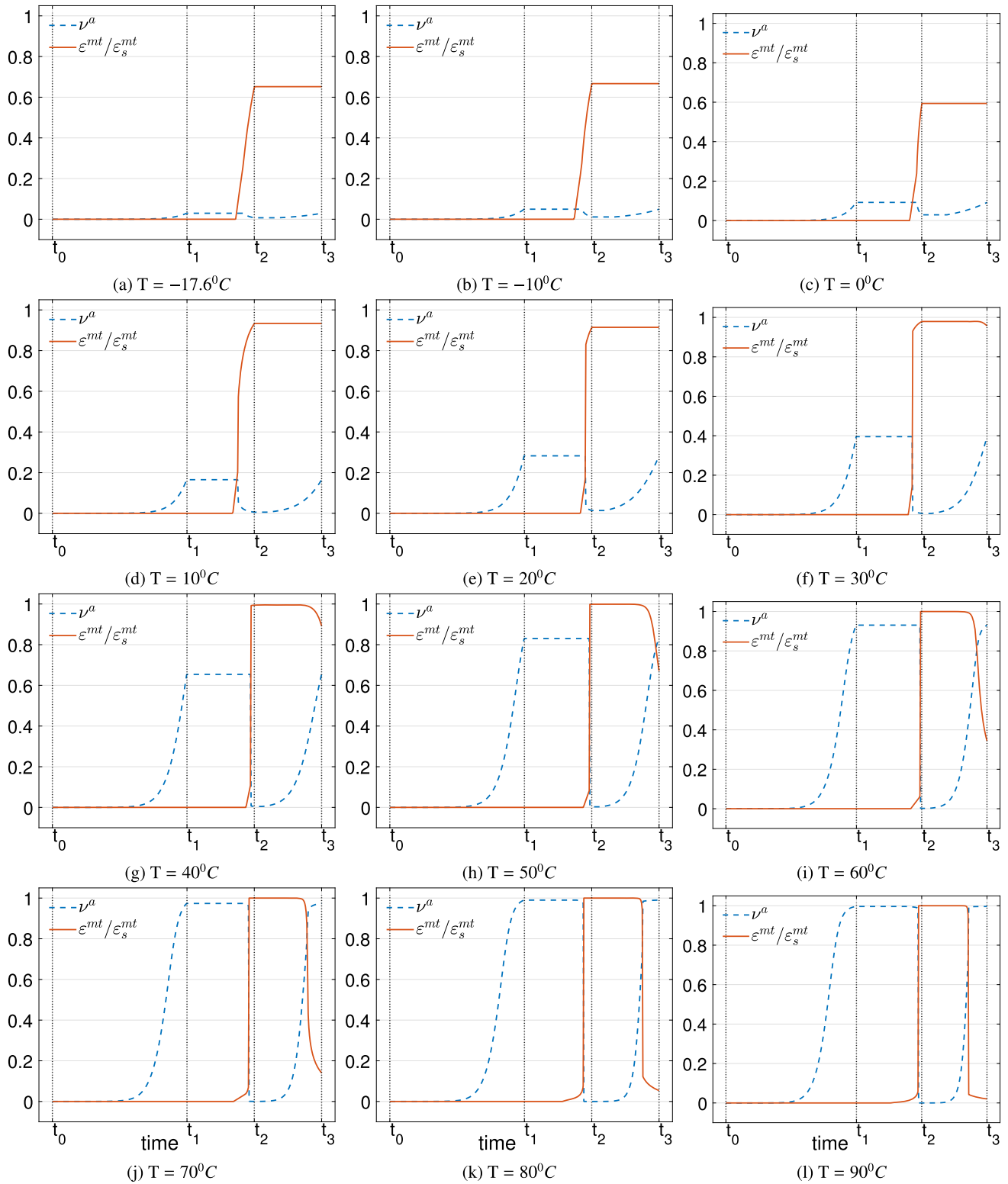


Figure 2. The evolution of internal variables v^a and normalised transformation strain ($\epsilon^{mt}/\epsilon_s^{mt}$) during uniaxial tensile loading at constant temperatures ranging from -17.6°C to 90°C .

tested for stress–strain behavior. This gives a significant difference in the stress–strain response. Quantitatively capturing such a variation in the response is essential in

complex thermomechanical loading conditions in actuator applications. Also, the model captures the difference in constitutive behavior during loading and unloading

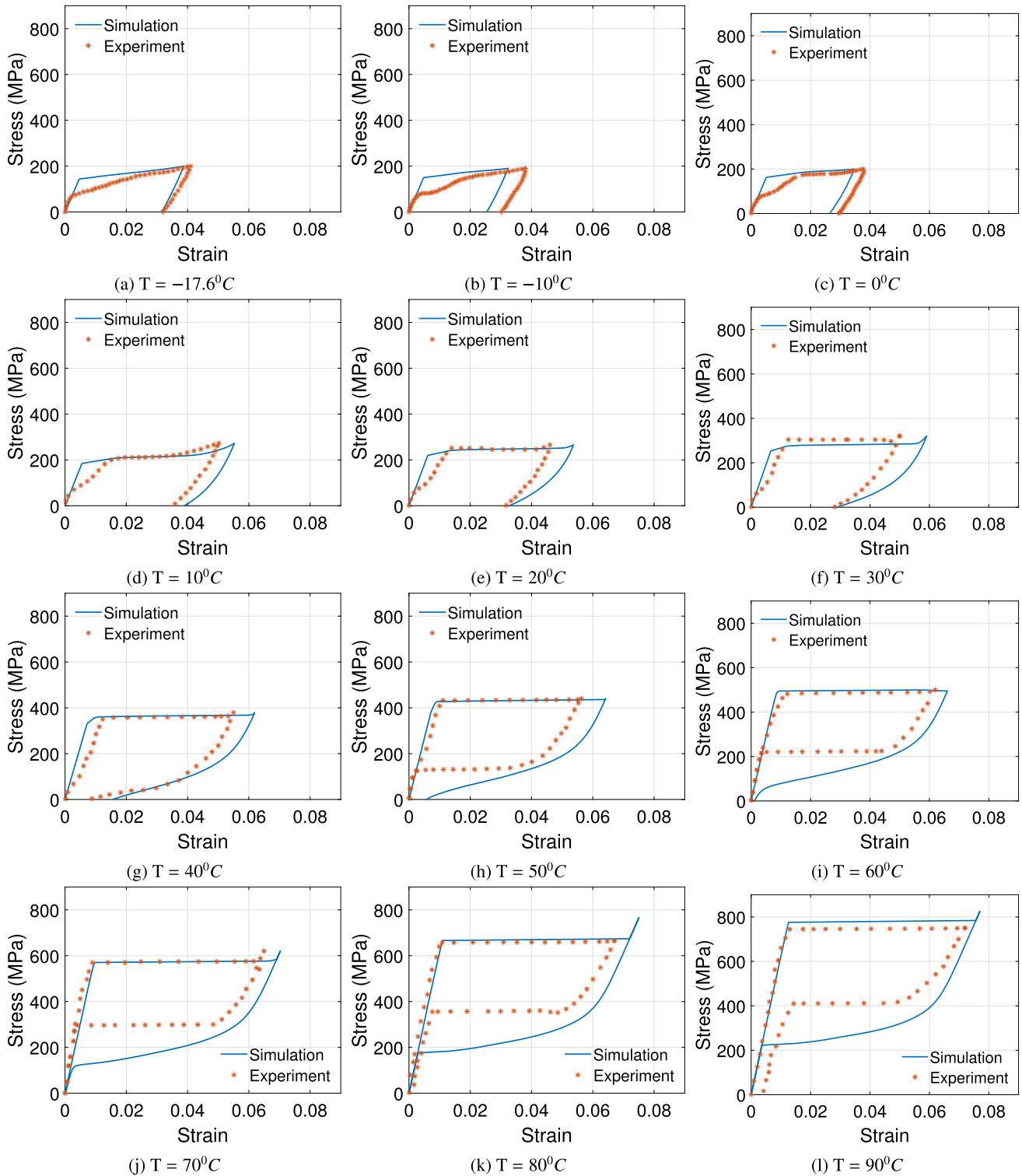


Figure 3. Uniaxial tensile stress–strain responses at temperatures ranging between -17.6°C and 90°C depicting two distinct behaviors of shape memory alloy. The solid line represents the analytical results, and the dotted line represents the experimental results [48].

reasonably well. This is achieved due to the presence of the inelastic martensite strain term in the yield function (ϕ^v) of the austenite volume fraction. In addition, the model also captures the stress plateau behavior identical to ideal plastic

material when it reaches the critical stress value. From the choice of σ_c as a function of v^a , the variation in the critical stress value at which the phase transformation happens is also captured with good approximation. The simulated

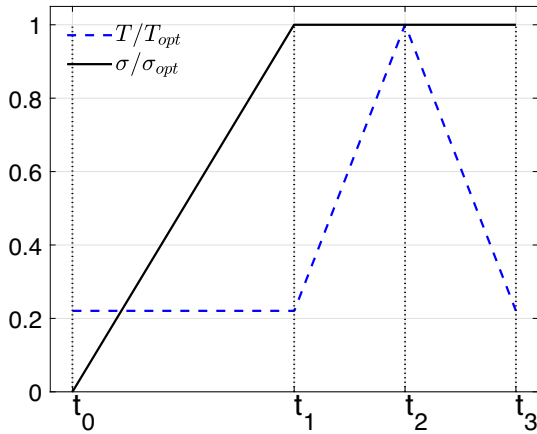


Figure 4. The thermal cyclic loading applied at constant stress from T_1 to T_3 for simulation the strain recovery during heating.

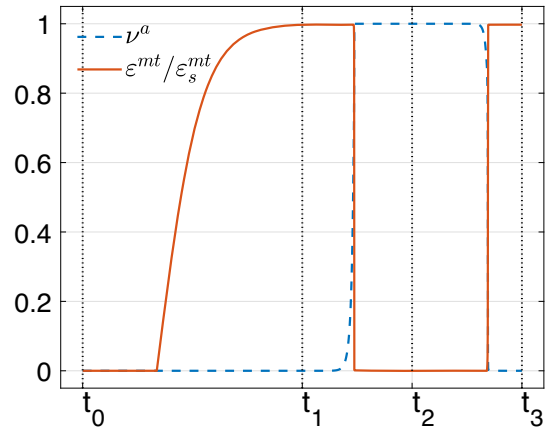


Figure 7. The evolution of internal variables v^a and $(\epsilon^{mt}/\epsilon_s^{mt})$ during thermal cyclic loading for $\sigma = 400$ MPa.

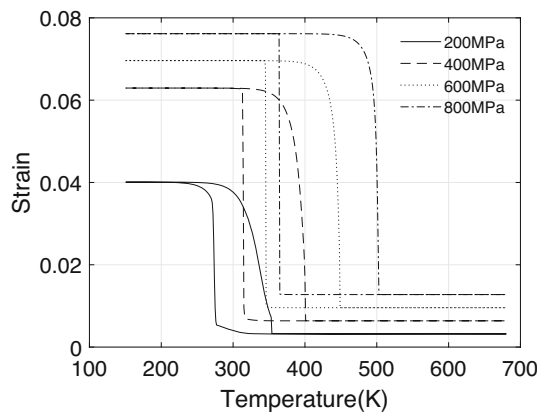


Figure 5. The simulation results of strain hysteresis observed during the thermal cycling at different constant stresses between 200 MPa and 800MPa.

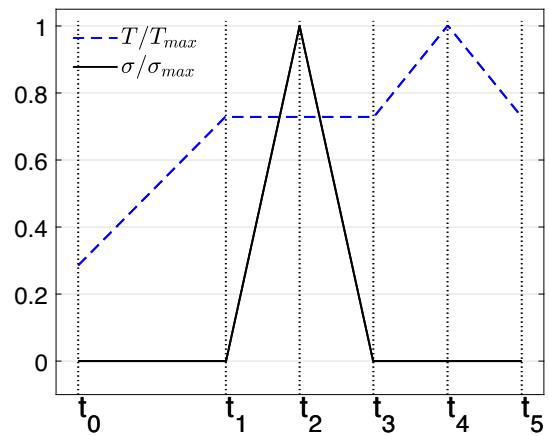


Figure 8. Thermomechanical loading applied to simulate the one-way shape memory effect.

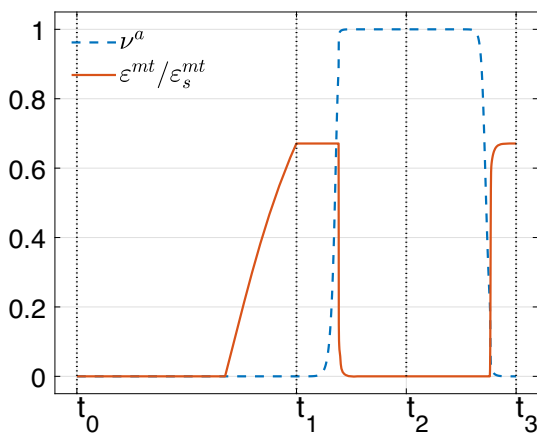


Figure 6. The evolution of internal variables v^a and $(\epsilon^{mt}/\epsilon_s^{mt})$ during thermal cyclic loading for $\sigma = 200$ MPa.

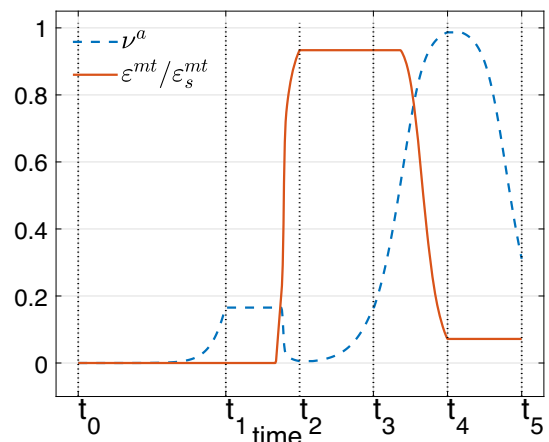


Figure 9. The evolution of internal variables v^a and $(\epsilon^{mt}/\epsilon_s^{mt})$ at 10°C describing the the one-way shape memory effect.

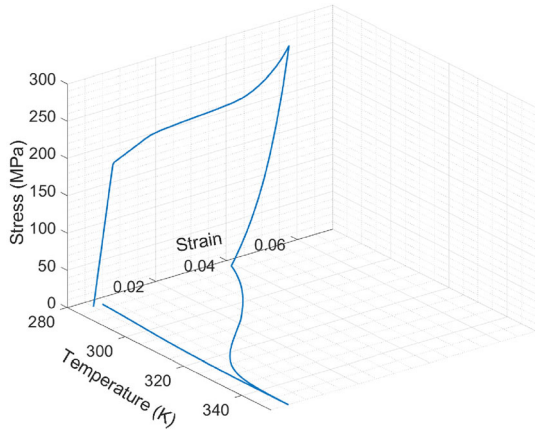


Figure 10. Shape memory effect at 10°C operating temperature.

strain value at σ_{max} also agrees reasonably with the experimental results.

5.2 Strain temperature hysteresis

This subsection discusses the simulation results of strain response for an increase and decrease in temperature under constant stress. Experimental studies of various SMA materials for such loading condition is vastly explored in the literature [49, 50]. These studies mainly characterize the material's ability to use as a thermally induced mechanical actuator. From the experimental results in the literature, it has been generally observed that the change in strain between the higher and lower temperatures increases as the stress increases within a certain range of stress values.

To simulate this behavior, the following thermomechanical loading condition is considered, see figure 4. At $t = t_0$, the material is assumed to be twinned martensite i.e. $v^a = 0$ and $\varepsilon^{mt} = 0$. At this low temperature, it is loaded until the desired stress is reached from t_0 to t_1 . This is followed by the thermal cycling between t_1 and t_3 , where the temperature increases to T_{opt} while maintaining the

stress value unchanged as shown in figure 4. The effect of detwinning can be observed through the evolution of inelastic martensite strain (ε^{mt}). For the applied load of 200 MPa, we can observe only the partial evolution of inelastic martensite strain as shown in figure 6. By increasing the load, the complete detwinning of martensite variants is achieved, which can be observed in figure 7. Similarly, the evolution of another internal variable, austenite volume fraction, increases up to t_2 along with temperature and decreases simultaneously. The detwinned martensite strain at the end loading (at t_1) is the available recoverable strain for actuation. As observed in figure 6 & 7 with the increase in the applied stress, the strain available is also increased. The total strain during the thermal cycling for various stress levels is given in figure 5.

5.3 Shape memory effect

The ability of the model to capture the entire behavior of the shape memory effect is discussed in this subsection. This complete behavior can be sequentially decomposed into the following behaviors. At first, the material undergoes an inelastic deformation providing the required transformation strain upon applied stress. Following that, the inelastic strain is recovered upon heating under stress-free conditions. During this process, the material transformed from martensite to austenite. Finally, upon cooling, the material remains undeformed and returns to the initial state completing the cycle.

To simulate this entire behavior, the loading condition given in figure 8 is considered. From t_0 to t_1 , the temperature is raised from a lower value to an operating value such that the material remains in the martensite phase. The austenite volume fraction can be noticed to have a near zero value, as seen in figure 9. This is followed by stress loading from t_1 to t_2 while keeping the temperature constant. During this loading condition, the material remains in the martensite phase. However, the inelastic martensite strain ε^{mt} increases near to ε_s^{mt} . This represents that the material

Table 3. Model parameters used in numerical simulations.

Parameter	NiTi Alloy [53]	NiTi Alloy [34] (54.8%Ni)	Cu-Zn-Sn Alloy [54] (63.5%Cu–33.3%Zn)	Unit
S_A	1/53600	1/32030	1/13898	MPa^{-1}
S_M	1/21100	1/18012	1/6831	MPa^{-1}
T_c	3	10	1.5	K
σ_c	$(1 - v) \times 250 + v \times 450$	$(1 - v) \times 120 + v \times 650$	$(1 - v) \times 12 + v \times 68$	MPa
T^0	250	350	350	K
c_1	0.7	0.7	0.8	$MPa K^{-1}$
c_2	4.1	4.1	11.2	–
ε_s^{mt}	0.05	0.04	0.01	–
a	35	35	9	MPa
b	5	4	0.5	K

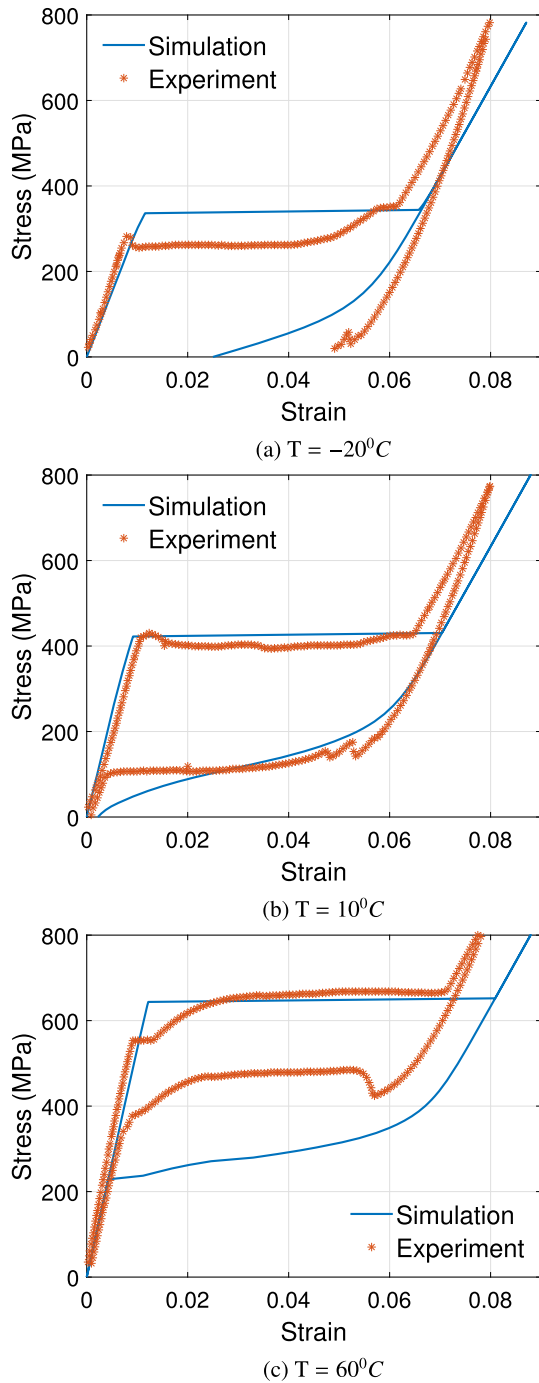


Figure 11. Comparison of simulation results with experiments performed on NiTi alloy by Sittner *et al* [53] for temperatures between -20°C to 60°C .

mostly converted from twinned to detwinned martensite. Upon unloading from t_2 to t_3 , the inelastic martensite strain remains the same in the material as observed in figure 9. The shape memory effect represents the recovery of this inelastic strain upon heating. In the interval between t_3 to t_4 , the loading curve shows the increase in temperature with zero stress. During this interval, the volume fraction of

austenite increases representing the reverse phase transformation. At the same time, ε^{mt} decreases simultaneously, causing the inelastic strain to recover. The complete strain recovery does not occur, leaving behind a permanent strain. This can be observed as the difference between inelastic martensite strain at t_1 & t_5 in figure 9. The cyclic behavior of SMA reveals that the evolution of permanent strain for virgin material stabilizes after certain cycles [51, 52]. The entire thermomechanical path can be observed in the temperature–stress–strain curve as shown in figure 10.

Further, upon cooling (t_4 to t_5), the material undergoes forward transformation changing its phase from austenite to twinned martensite. This phase change causes the decrease in the austenite volume fraction v^a while the ε^{mt} remains unchanged. The inelastic strain, which was recovered during the heating process, remains unchanged during the cooling process. This unchanged strain can also be seen in figure 9. Thus, it can be seen that the proposed model can completely capture the shape memory effect of the material.

5.4 Stress strain response for other SMA alloys

The behavior of shape memory alloy is understood to be dependent on the composition of the alloy and the thermomechanical processing it has undergone [55]. They dictate the transformation temperatures, pseudoelasticity, and shape memory effect of the alloy. The model must be able to capture the variations of different classes effectively. To show the robustness of the model within the same framework, the model parameters are identified for different classes of SMA materials to capture its stress–strain behavior. In order to do this, the experimental data from the following literature are considered [34, 53, 54]. The thermomechanical loading similar to the one discussed in section (5.1) is used. The material parameter for each shape memory alloy is tabulated and given in table 3. Figure 11, 12, 13 shows the comparison between the experimental data and the simulation results at various temperatures. By observing these experimental data, it is evident that the stress–strain curves are distinguishable between each material concerning the shape. The simulation results show that this difference can be easily captured with the proposed model.

6. Conclusion

A new stress-based phenomenological constitutive model is proposed for modeling the complex behavior of shape memory alloy. This model provides a novel framework to describe the forward, reverse transformation, and detwinning of martensite without the need to know the load a priori. To perform the numerical implementation of the

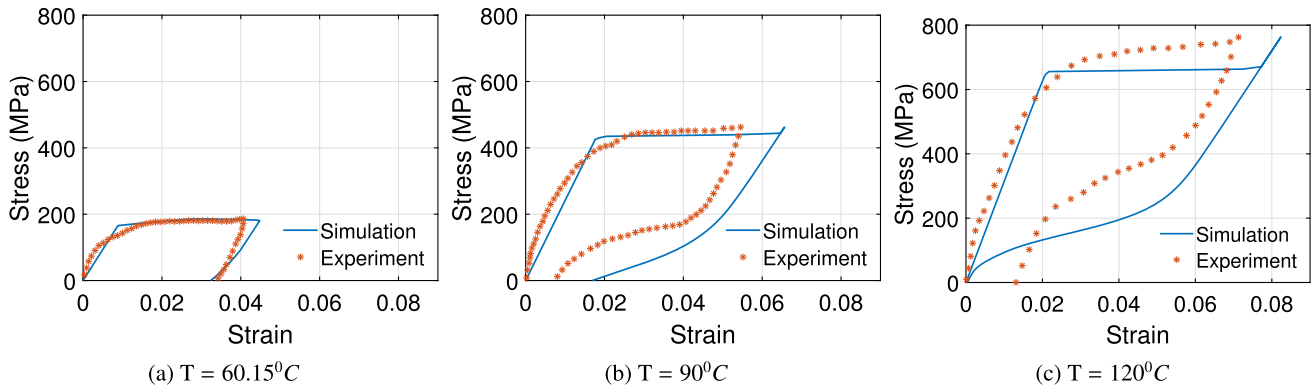


Figure 12. Comparison of simulation results with experiments performed on NiTi alloy by Woodworth *et al* [34] for temperatures between 60°C. to 120°C

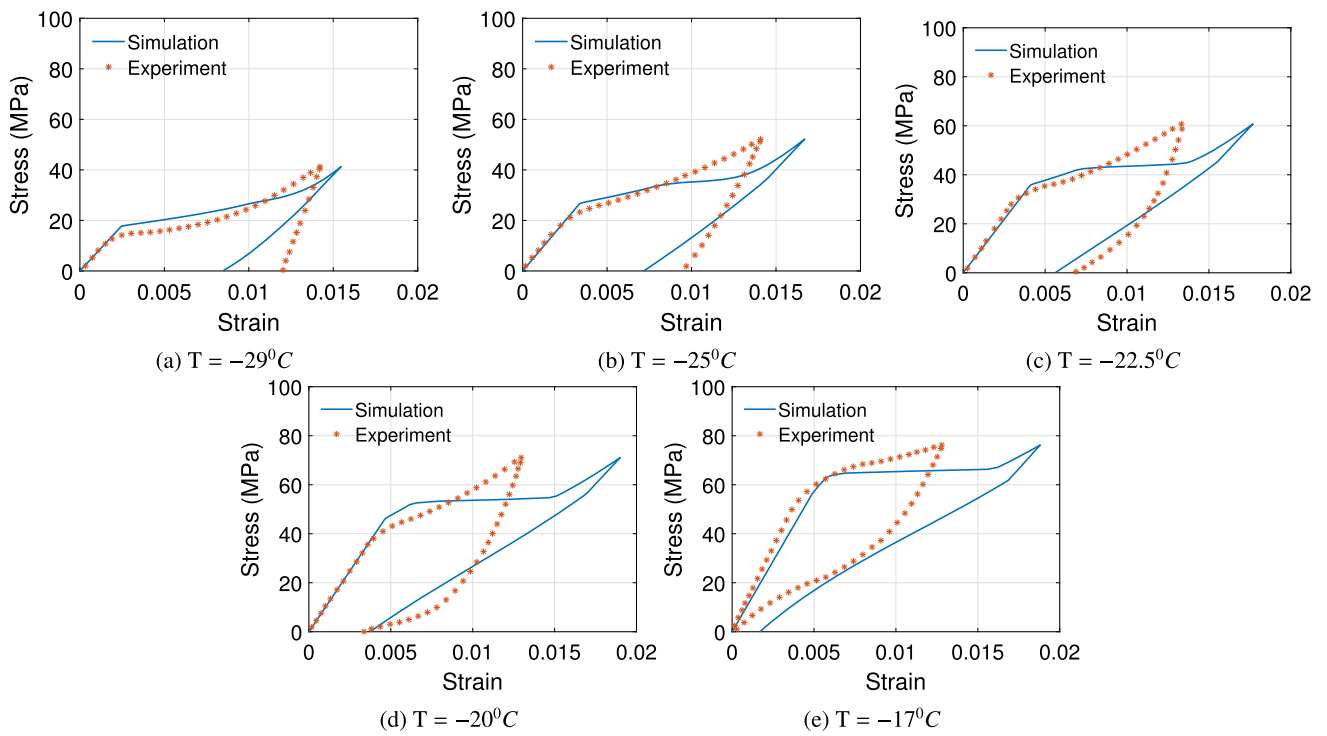


Figure 13. Comparison of simulation results with experiments performed on Cu-Zn-Sn alloy by Eisenwasser and Brown [54] for temperatures between $-29^{\circ}C$ to $-17^{\circ}C$.

proposed model, the algorithmic procedure has been given. The efficacy of the model is discussed by subjecting it to different thermomechanical loading conditions. By comparing it with the experimental data from the literature, it is shown that the model can effectively capture the gradual variation between pseudoelasticity and shape memory effect of the NiTi alloy. The model also captures the partial recovery of the inelastic strain during the initial loading cycles. Further, it is shown that the framework work can be adopted for modeling the behavior of different classes of alloys by changing the model parameters. These features make the proposed model an important tool for modeling

the mechanisms utilizing SMA wire. This framework, along with a minimal set of variables, helps in the effective integration of the model in applications. Based on this work, it can be extended to simulate the three-dimensional loading conditions for complex applications.

Acknowledgements

This work was supported by a grant from Science and Engineering Research Board (SERB) under the SRG program, Project no.: SRG/2021/001672. The authors

would also like to thank Dr. Ratna Kumar Annabattula from IITM Chennai for the fruitful discussions regarding this work.

References

- [1] Saburi T 1998 Ti-Ni shape memory alloys. In: *Shape memory materials*, pp. 49–96
- [2] Duerig T W, Melton K N, and Stöckel D 2013 *Engineering Aspects of Shape Memory Alloys* Butterworth-Heinemann,
- [3] Jani J M, Leary M, Subic A and Gibson M A 2014 A review of shape memory alloy research, applications and opportunities. *Mater. Design* 56: 1078–1113
- [4] Lorenza Petrini and Francesco Migliavacca 2011 Biomedical applications of shape memory alloys. *J. Metall.* 2011: e501483
- [5] Jeya Ganesh N, Maniprakash S, Chandrasekaran L, Srinivasan S M, and Srinivasa A R 2011 Design and development of a sun tracking mechanism using the direct SMA actuation *J. Mech. Design*, 133(7)
- [6] Saeed Akbari Amir, Hosein Sakhaei, Sahil Panjwani, Kavin Kowsari and Qi Ge 2021 Shape memory alloy based 3D printed composite actuators with variable stiffness and large reversible deformation. *Sens. Actuators A: Phys.* 321: 112598
- [7] Ali Hussein F M, Manan Khan Abdul, Hangyeol Baek, Buhyun Shin and Youngshik Kim 2021 Modeling and control of a finger-like mechanism using bending shape memory alloys. *Microsyst. Technol.* 27(6): 2481–2492
- [8] Fares Maimani, Calderón Ariel A, Xiufeng Yang, Alberto Rigo, Ge Joey Z and Pérez-Arancibia Néstor O 2022 A 7-mg miniature catalytic-combustion engine for millimeter-scale robotic actuation. *Sens. Actuators A: Phys.* 341: 112818
- [9] Mohammadreza Lalegani Dezaki, Mahdi Bodaghi, Ahmad Serjouei, Shukri Afazov and Ali Zolfagharian 2022 Adaptive reversible composite-based shape memory alloy soft actuators. *Sens. Actuators A: Phys.* 345: 113779
- [10] Cheikh Cisse, Wael Zaki and Tarak Ben Zineb 2016 A review of constitutive models and modeling techniques for shape memory alloys. *Int. J. Plast.* 76: 244–284
- [11] Ashish Khandelwal and Vidyashankar Buravalla 2009 Models for shape memory alloy behavior: an overview of modeling approaches. *Int. J. Struct. Changes Solids* 1(1): 111–148
- [12] Alberto Paiva and Amorim Savi Marcelo 2006 An overview of constitutive models for shape memory alloys. *Math. Probl. Eng.* 2006: e56876
- [13] Kikuaki Tanaka, Shigenori Kobayashi and Yoshio Sato 1986 Thermomechanics of transformation pseudoelasticity and shape memory effect in alloys. *Int. J. Plast.* 2(1): 59–72
- [14] Liang C and Rogers C A 1990 One-dimensional thermomechanical constitutive relations for shape memory materials. *J. Intell. Mater. Syst. Struct.* 8(4): 285–302
- [15] Brinson L C 1993 One-dimensional constitutive behavior of shape memory alloys: thermomechanical derivation with non-constant material functions and redefined martensite internal variable: *J. Intell. Mater. Syst. Struct.*
- [16] Banerjee A 2012 Simulation of shape memory alloy wire actuator behavior under arbitrary thermo-mechanical loading. *Smart Mater. Struct.* 21(12): 125018
- [17] Jarali Chetan S, Chikkangoudar Ravishankar N, Patil Subhas F, Raja S, Lu Charles Y, and Fish Jacob 2019 Thermodynamically consistent approach for one-dimensional phenomenological modeling of shape memory alloys *Int. J. Multiscale Comput. Eng.*, 17(4)
- [18] Arthur Adeodato, Vignoli Lucas L, Alberto Paiva, Monteiro Luciana L S, Pacheco Pedro M C L and Savi Marcelo A 2022 A shape memory alloy constitutive model with polynomial phase transformation kinetics. *Shape Memory Superelasticity* 8(4): 277–294
- [19] Auricchio F and Lubliner J 1997 A uniaxial model for shape-memory alloys. *Int. J. Solids Struct.* 34(27): 3601–3618
- [20] Panoskaltzis V P, Bahuguna S and Soldatos D 2004 On the thermomechanical modeling of shape memory alloys. *Int. J. Non-Linear Mech.* 39(5): 709–722
- [21] Souza Angela C, Mamiya Edgar N and Nestor Zouain 1998 Three-dimensional model for solids undergoing stress-induced phase transformations. *Eur. J. Mech. A/Solids* 17(5): 789–806
- [22] Ferdinando Auricchio and Lorenza Petrini 2004 A three-dimensional model describing stress-temperature induced solid phase transformations: solution algorithm and boundary value problems. *Int. J. Numerical Methods Eng.* 61(6): 807–836
- [23] Boyd J G and Lagoudas D C 1996 A thermodynamical constitutive model for shape memory materials Part I. The monolithic shape memory alloy. *Int. J. Plast.* 12(6): 805–842
- [24] Qidwai M A and Lagoudas D C 2000 On thermomechanics and transformation surfaces of polycrystalline NiTi shape memory alloy material. *Int. J. Plast.* 16(10): 1309–1343
- [25] Peter Popov and Lagoudas Dimitris C 2007 A 3-D constitutive model for shape memory alloys incorporating pseudoelasticity and detwinning of self-accommodated martensite. *Int. J. Plast.* 23(10–11): 1679–1720
- [26] Auricchio F, Bonetti E, Scalet G and Ubertini F 2014 Theoretical and numerical modeling of shape memory alloys accounting for multiple phase transformations and martensite reorientation. *Int. J. Plast.* 59: 30–54
- [27] Zhixiang Rao, Jiaming Leng, Zehong Yan, Limeng Tan and Xiaojun Yan 2023 A three-dimensional constitutive model for shape memory alloy considering transformation-induced plasticity, two-way shape memory effect, plastic yield and tension-compression asymmetry. *Eur. J. Mech. A/Solids* 99: 104945
- [28] Dimitris Chatziathanasiou, Yves Chemisky, George Chatzigeorgiou and Fodil Meraghni 2016 Modeling of coupled phase transformation and reorientation in shape memory alloys under non-proportional thermomechanical loading. *Int. J. Plast.* 82: 192–224
- [29] Guillaume Helbert, Luc Saint-Sulpice, Shabnam Arbab Chirani, Lamine Dieng, Thibaut Lecompte, Sylvain Calloch and Philippe Pilvin 2014 Experimental characterisation of three-phase NiTi wires under tension. *Mech. Mater.* 79: 85–101
- [30] Frost M, Jury A, Heller L and Sedláček P 2021 Experimentally validated constitutive model for NiTi-based shape memory alloys featuring intermediate R-phase transformation: A case study of Ni₄₈Ti₄₉Fe₃. *Mater. Design* 203: 109593
- [31] Longfei Wang, Peihua Feng, Xuegang Xing, Ying Wu and Zishun Liu 2021 A one-dimensional constitutive model for NiTi shape memory alloys considering inelastic strains

- caused by the R-phase transformation. *J. Alloys Compd.* 868: 159192
- [32] Jan Frenzel 2020 On the importance of structural and functional fatigue in shape memory technology. *Shape Memory Superelasticity* 6(2): 213–222
- [33] Dornelas Vanderson M, Oliveira Sergio A, Savi Marcelo A, Lopes Pacheco Pedro Manuel Calas and Souza de Luis Felipe G 2021 Fatigue on shape memory alloys: experimental observations and constitutive modeling. *Int. J. Solids Struct.* 213: 1–24
- [34] Woodworth Lucas A, Felix Lohse, Karl Kopelmann, Chokri Cherif and Michael Kaliske 2022 Development of a constitutive model considering functional fatigue and pre-stretch in shape memory alloy wires. *Int. J. Solids Struct.* 234–235: 111242
- [35] Alsawalhi Mohammed Y and Landis Chad M 2022 A new phenomenological constitutive model for shape memory alloys. *Int. J. Solids Struct.* 257: 111264
- [36] Grabe C and Bruhns O T 2008 On the viscous and strain rate dependent behavior of polycrystalline NiTi. *Int. J. Solids Struct.* 45(7): 1876–1895
- [37] Claire Morin, Ziad Moumni and Wael Zaki 2011 Thermo-mechanical coupling in shape memory alloys under cyclic loadings: Experimental analysis and constitutive modeling. *Int. J. Plast.* 27(12): 1959–1980
- [38] Mingzhao Zhuo 2020 Timescale competition dictates thermo-mechanical responses of niti shape memory alloy bars. *Int. J. Solids Struct.* 193–194: 601–617
- [39] Hartl Darren J, George Chatzigeorgiou and Lagoudas Dimitris G 2010 Three-dimensional modeling and numerical analysis of rate-dependent irrecoverable deformation in shape memory alloys. *Int. J. Plast.* 26(10): 1485–1507
- [40] Ashwin Rao, Annie Ruimi and Srinivasa Arun R 2014 Internal loops in superelastic shape memory alloy wires under torsion—experiments and simulations/predictions. *Int. J. Solids Struct.* 51(25): 4554–4571
- [41] Viet N V, Zaki W, Umer R and Xu Y 2020 Mathematical model for superelastic shape memory alloy springs with large spring index. *Int. J. Solids Struct.* 185–186: 159–169
- [42] Hamid Khodaei and Patrick Terriault 2018 Experimental validation of shape memory material model implemented in commercial finite element software under multiaxial loading. *J. Intell. Mater. Syst. Struct.* 29(14): 2954–2965
- [43] Nallathambi Ashok K, Doraiswamy Srikrishna, Chandrasekar A S and Srinivasan Sivakumar M 2009 A 3-species model for shape memory alloys. *Int. J. Struct. Changes Solids* 1(1): 149–170
- [44] Karakalas A, Machairas T, Solomou A, and Saravanos D 2017 Effect of shape memory alloy partial transformation on the performance of morphing wind turbine airfoils. In: *28th International Conference on Adaptive Structures and Technologies, ICAST*
- [45] Coleman Bernard D and Gurtin Morton E 1967 Thermodynamics with internal state variables. *J. Chem. Phys.* 47(2): 597–613
- [46] Klinkel S 2006 A phenomenological constitutive model for ferroelastic and ferroelectric hysteresis effects in ferroelectric ceramics. *Int. J. Solids Struct.* 43(22–23): 7197–7222
- [47] Miehe C and Rosato D 2011 A rate-dependent incremental variational formulation of ferroelectricity. *Int. J. Eng. Sci.* 49(6): 466–496
- [48] Shaw John A and Stelios Kyriakides 1995 Thermomechanical aspects of NiTi. *J. Mech. Phys. Solids* 43(8): 1243–1281
- [49] Wu X D, Sun G J and Wu J S 2003 The nonlinear relationship between transformation strain and applied stress for nitinol. *Mater. Lett.* 57(7): 1334–1338
- [50] Sivom Manchiraju, Darrell Gaydosh, Othmane Benafan, Ronald Noebe, Raj Vaidyanathan and Anderson Peter M 2011 Thermal cycling and isothermal deformation response of polycrystalline NiTi: simulations versus experiment. *Acta Materialia* 59(13): 5238–5249
- [51] Ashrafi M J 2019 Constitutive modeling of shape memory alloys under cyclic loading considering permanent strain effects. *Mech. Mater.* 129: 148–158
- [52] Bingfei Liu, Shangyang Jin, Keying Chen, Fusheng Wang and Chunzhi Du 2019 Study on cyclic deformation behavior of shape memory alloy materials considering damage and the residual strain. *J. Alloys Compd.* 797: 1142–1150
- [53] Sittner P, Heller L, Pilch J, Sedlak P, Frost M, and Chemisky Y *et al* 2009 Roundrobin SMA modeling. In: *ESOMAT 2009 - 8th European Symposium on Martensitic Transformations*, p. 08001
- [54] Eisenwasser J D and Brown L C 1972 Pseudoelasticity and the strain-memory effect in Cu-Zn-Sn alloys. *Metall. Trans.* 3(6): 1359–1363
- [55] Saleeb A F, Dhakal B, Dilibal S, Owusu-Danquah J S and Padula S A 2015 On the modeling of the thermo-mechanical responses of four different classes of NiTi-based shape memory materials using a general multi-mechanism framework. *Mech. Mater.* 80: 67–86

Springer Nature or its licensor (e.g. a society or other partner) holds exclusive rights to this article under a publishing agreement with the author(s) or other rightsholder(s); author self-archiving of the accepted manuscript version of this article is solely governed by the terms of such publishing agreement and applicable law.